

## Haline hurricane wake in the Amazon/Orinoco plume: AQUARIUS/SACD and SMOS observations

Semyon A. Grodsky,<sup>1</sup> Nicolas Reul,<sup>2</sup> Gary Lagerloef,<sup>3</sup> Gilles Reverdin,<sup>4</sup> James A. Carton,<sup>1</sup>  
Bertrand Chapron,<sup>2</sup> Yves Quilfen,<sup>2</sup> Vladimir N. Kudryavtsev,<sup>5,6</sup> and Hsun-Ying Kao<sup>3</sup>

Received 30 July 2012; revised 5 September 2012; accepted 10 September 2012; published 18 October 2012.

[1] At its seasonal peak the Amazon/Orinoco plume covers a region of  $10^6$  km<sup>2</sup> in the western tropical Atlantic with more than 1 m of extra freshwater, creating a near-surface barrier layer (BL) that inhibits mixing and warms the sea surface temperature (SST) to  $>29^\circ\text{C}$ . Here new sea surface salinity (SSS) observations from the Aquarius/SACD and SMOS satellites help elucidate the ocean response to hurricane Katia, which crossed the plume in early fall, 2011. Its passage left a 1.5 psu high haline wake covering  $>10^5$  km<sup>2</sup> (in its impact on density, the equivalent of a  $3.5^\circ\text{C}$  cooling) due to mixing of the shallow BL. Destruction of this BL apparently decreased SST cooling in the plume, and thus preserved higher SST and evaporation than outside. Combined with SST, the new satellite SSS data provide a new and better tool to monitor the plume extent and quantify tropical cyclone upper ocean responses with important implications for forecasting. **Citation:** Grodsky, S. A., N. Reul, G. Lagerloef, G. Reverdin, J. A. Carton, B. Chapron, Y. Quilfen, V. N. Kudryavtsev, and H.-Y. Kao (2012), Haline hurricane wake in the Amazon/Orinoco plume: AQUARIUS/SACD and SMOS observations, *Geophys. Res. Lett.*, *39*, L20603, doi:10.1029/2012GL053335.

### 1. Introduction

[2] Because of the importance of latent heat release as an energy source, hurricane strength depends on changes in the underlying ocean thermal stratification [e.g., *Shay et al.*, 2000; *Saunders and Lea*, 2008]. Intense hurricane-induced mixing and upwelling act to entrain cool thermocline water into the mixed layer, leaving behind a cool wake of SST depressed by a few degrees, which reduces hurricane growth potential [e.g., *Price*, 1981; *Bender and Ginis*, 2000;

*Zhu and Zhang*, 2006]. Passage over freshwater plumes generally causes strengthening of hurricanes due to high SST [*Ffield*, 2007; *Vizy and Cook*, 2010] and minimization of the cool wake due to the presence of the BL [*Sengupta et al.*, 2008; *Wang et al.*, 2011; *Balaguru et al.*, 2012]. These produce nearly 50% increase in intensification rate over BL regions and occur in 10–20% of tropical cyclone cases worldwide [*Balaguru et al.*, 2012], but are more probable (68%) for the most intense (category 5) hurricanes [*Ffield*, 2007]. Here we combine newly available SSS from the Aquarius/SACD and SMOS missions together with other in situ and remote sensing observations to explore the impact of the Amazon/Orinoco plume on spatial and temporal signatures of SSS and SST after the passage of hurricane Katia in fall, 2011. We expect that new ability to map the plume more precisely with satellite SSS will benefit hurricane forecasting when it is evident that the trajectory will intersect the plume at some stage.

[3] Unlike SST widely available from remote sensing, SSS is relatively sparse and its response to passing storms is often overlooked. Recognition of the impact of hurricane on a BL goes back at least to sample profile observations of *Price* [1981] showing the breakdown of a BL in the Gulf of Mexico. A similar Argo record was presented by *McPhaden et al.* [2009] in the Bay of Bengal. But, compared to ARGO or moorings, the satellite SSS now enables tracking the spatial variability of SSS induced by hurricanes in an unprecedented manner.

[4] The western tropical Atlantic is characterized by high SST  $> 29^\circ\text{C}$ , and a plume of low SSS caused by Amazon and to a lesser extent Orinoco river discharge as well as local rainfall [*Yoo and Carton*, 1990; *Dessier and Donguy*, 1994; *Lentz*, 1995; *Foltz and McPhaden*, 2008]. This freshwater forcing produces a strong halocline in the upper 3–30 m, below which salinity exceeds 36 psu. The plume deepens seaward and acts as a BL in density whose presence is associated with elevated SST [*Pailler et al.*, 1999; *Mignot et al.*, 2012]. The plume extends eastward from the mouth of the Amazon at  $0\text{--}2^\circ\text{N}$ ,  $50^\circ\text{W}$  with widths of 200–300 km in June through December when Amazon discharge is at a seasonal minimum ( $0.08 \times 10^6$  m<sup>3</sup>/s in November), expanding to 400–500 km in March to May when Amazon discharge reaches a seasonal maximum of  $0.24 \times 10^6$  m<sup>3</sup>/s and winds are weak [*Hu et al.*, 2004; *Salisbury et al.*, 2011]. At this rate of discharge an area of  $10^6$  km<sup>2</sup> is diluted by 2 psu down to the 20 m depth in around two months. Further north the seasonality of the plume is the reverse in that it reaches its maximum northward and eastward extent from the coast in August–September when the zone of weak winds shifts northward. The plume contracts in November,

<sup>1</sup>Department of Atmospheric and Oceanic Science, University of Maryland, College Park, Maryland, USA.

<sup>2</sup>Institut Français pour la Recherche et l'Exploitation de la Mer, Plouzane, France.

<sup>3</sup>Earth and Space Research, Seattle, Washington, USA.

<sup>4</sup>Laboratoire d'Océanographie et de Climatologie par Expérimentation et Analyse Numérique, Institut Pierre Simon Laplace, CNRS/UPMC/IRD/MNHN, Paris, France.

<sup>5</sup>Satellite Oceanography Laboratory, Russian State Hydrometeorological University, St. Petersburg, Russia.

<sup>6</sup>Nansen International Environmental and Remote Sensing Centre, St. Petersburg, Russia.

Corresponding author: S. A. Grodsky, Department of Atmospheric and Oceanic Science, University of Maryland, College Park, MD 20742, USA. (senya@atmos.umd.edu)

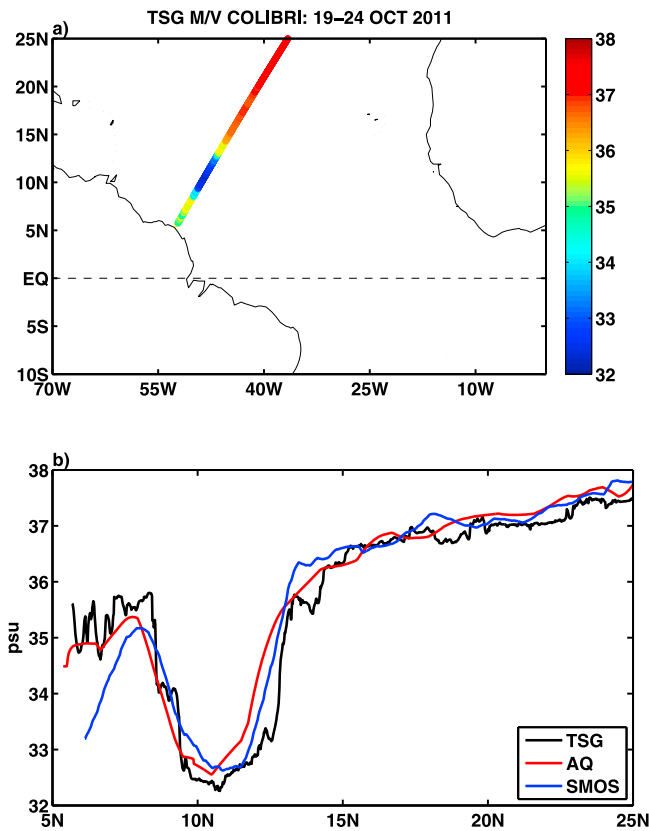


**Figure 1.** (a) Thermosalinograph (TSG) transect along Europe-French Guiana shipping route collected by vessel COLIBRI. Color indicates value of salinity. (b) TSG data with collocated weekly running mean AQUARIUS (AQ) and SMOS SSS.

which is coincident with the reappearance of the northeast trade winds and shifts in the surface currents [Dessier and Donguy, 1994].

[5] The hurricane season in the Atlantic extends from early June through the end of November, with a peak in late August - early September. The most intense hurricanes, according to the National Hurricane Center (NHC), form off the Cape Verde Islands in the eastern basin in fall, growing as they progress westward across the warm SSTs. In 2011, the first of two Cape Verde hurricanes and the second hurricane of the season began as tropical storm, Katia, in late August. Katia reached a Category 1 on September 1 with minimum central pressure of  $P_{\min} = 988$  mb and the radius of sustained hurricane force winds  $R = 55$  km. By the afternoon of September 4, Katia reached a Category 2 (maximum sustained winds  $>44$  m/s,  $P_{\min} = 961$  mb, and  $R = 75$  km). By the evening of September 5, after passing over the freshwater plume, Katia had strengthened to a Category 4 (winds  $>60$  m/s,  $P_{\min} = 942$  mb, and  $R = 95$  km). Twenty-four hours later, Katia weakened to a Category 1. Here we examine the response of the upper ocean to the passage of Katia as it appears in the in situ and satellite records.

## 2. Data

[6] SSS is provided by US/Argentina Aquarius/SACD [Lagerloef et al., 2008; Lagerloef, 2012; Lagerloef et al.,

2012] and the ESA Soil Moisture and Ocean Salinity (SMOS) [Reul et al., 2012a] missions. Aquarius daily L3 SSS (<ftp://saltmarsh.jpl.nasa.gov/L3/mapped/V1.3>) is available since 25 August, 2011 and provides global coverage every week on a  $1^\circ \times 1^\circ$  grid. Higher resolution  $0.2^\circ \times 0.2^\circ$  bias corrected SSS [Lagerloef, 2012; Lee et al., 2012] is compiled for two weeks encompassing the passage of Katia. SMOS was launched in November, 2009. It has average resolution of 43 km and provides global coverage every 3 days. Here we use L3 SMOS SSS from ‘Centre Aval de Traitement des Données SMOS’ (CATDS, [www.catds.fr](http://www.catds.fr), see documentation at [www.salinityremotesensing.ifremer.fr/documentation-cec-products](http://www.salinityremotesensing.ifremer.fr/documentation-cec-products)).

[7] Both sensors operate in the 21 cm microwave L-band and thus sample salinity in the upper few centimeters of the ocean. Since surface roughness strongly affects L-band brightness temperature [Lagerloef et al., 2008; Reul et al., 2012a], and SMOS does not measure it, SSS is estimated with a 1 to 2 days lag after hurricane passage to allow the sea state to calm. Despite this roughness-dependence, L-band frequencies have a compensating advantage in that they are less affected by clouds and rain than higher frequencies, and thus can be used to infer stormy winds [Reul et al., 2012b].

[8] The accuracy of the 10-day SMOS SSS is  $\sim 0.3$  psu in the tropics [Reul et al., 2012a]. The accuracy of Aquarius SSS is assessed in the auxiliary material by comparison to in situ  $\sim 1$  m depth salinity from the Indian, Atlantic, and Pacific tropical moorings, during August, 2011–May, 2012.<sup>1</sup> RMS difference of weekly Aquarius SSS is  $<0.25$  psu, with a slight 0.1 psu negative bias relative to in situ salinity. The bias is stronger in regions of low SSS, as expected, where intense rainfall produces the freshwater lenses [Henocq et al., 2010; Reverdin et al., 2012]. Comparison of the much more limited set of 121 spatially and temporally collocated Argo and Aquarius during September to November, 2011 suggests a somewhat larger range of differences. Prior to its use in this study the temporal variations of Aquarius SSS averaged zonally and with latitude in the band  $50^\circ\text{S}–50^\circ\text{N}$  are removed to lessen the impact of a known 0.2 psu time-dependent bias (due to an unaccounted for component of radiometer drift (D. Levine, personal communication, 2012)). To increase stability and accuracy we only use weekly average Aquarius SSS.

[9] Figure 1 illustrates a comparison of the two satellite SSSs with in situ 5 m depth thermosalinograph (TSG) along a ship track passing through 500 km of the Amazon plume ( $8^\circ–13^\circ\text{N}$ ) during which the intake salinity drops by 3–4 psu to well below 34 psu. The coincident satellite SSSs show a similar signature of the plume, although displaced slightly southward (however this apparent shift may result from the SSS spatial and temporal averaging).

[10] In addition to SSS we examine daily SST based on satellite microwave and infrared and in-situ data, available at  $0.25^\circ \times 0.25^\circ$  resolution [Reynolds et al., 2007] and TRMM Microwave Imager (TMI) SST ([www.ssmi.com/tmi/tmi\\_browse.html](http://www.ssmi.com/tmi/tmi_browse.html)). Daily  $0.25^\circ \times 0.25^\circ$  L3 Advanced SCATterometer (ASCAT) 10 m neutral winds of Bentamy and Croize-Fillon [2012] are available at <ftp.ifremer.fr/ifremer/cersat/products/gridded/MWF>. In-situ vertical profiles

<sup>1</sup>Auxiliary materials are available in the HTML. doi:10.1029/2012GL053335.

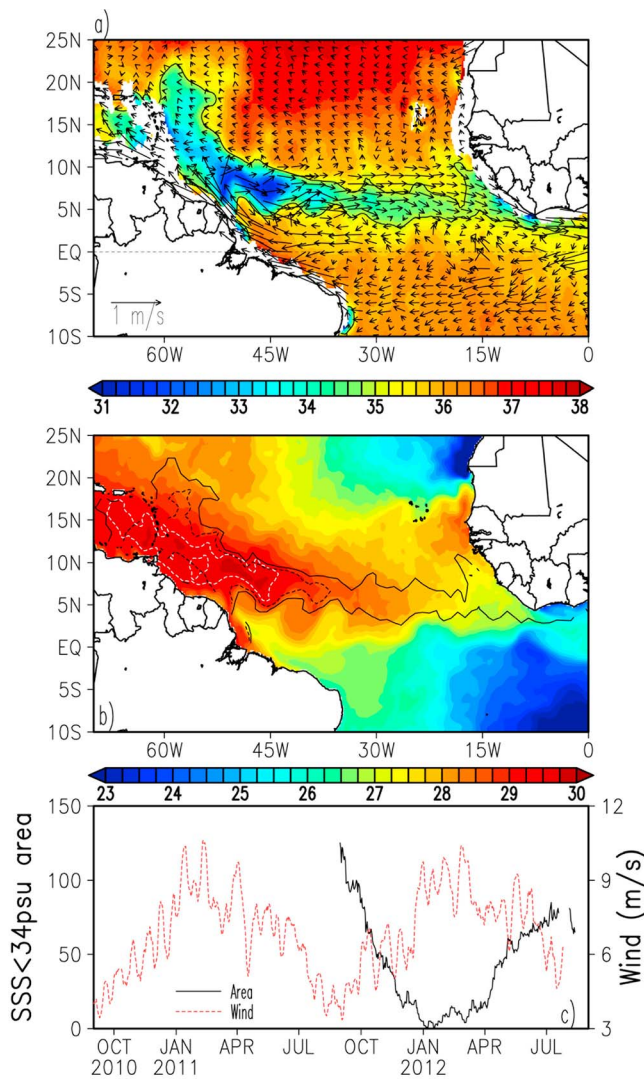


**Figure 2.** September 2011 mean (a) AQUARIUS SSS (shaded, psu) with September surface currents of *Lumpkin and Garraffo* [2005] overlain and (b) SST (shaded, degC), 34 psu (dashed, black) and 35 psu (solid, black) contours are overlain, ‘hot spots’ SST > 29.5C are emphasized. (c) Fresh water area (number of  $1^\circ \times 1^\circ \text{ deg}^2$  boxes within 34 psu contour) and winds averaged over the September 2011 SSS < 34 psu area (shown in Figure 2b). Land-contaminated coastal data are blanked.

of temperature and salinity are provided by the Argo Program [Roemmich *et al.*, 2009].

### 3. Results

[11] During our records (Figure 2a), the region of low SSS < 34 psu in the plume has a maximum area  $>10^6 \text{ km}^2$  extending northward to  $20^\circ\text{N}$  and westward into the Caribbean (partly due to the contribution of the Orinoco), and is mainly confined to regions where SST >  $29^\circ\text{C}$  (Figure 2b). The plume extends eastward to  $40^\circ\text{W}$  along the North Equatorial Countercurrent in the latitude band  $5^\circ\text{--}10^\circ\text{N}$ . It is separated from the coast by a few hundred kilometers wide patch of higher salinity evident along the transect in Figure 1. This plume differs from the September climatology of

*Dessier and Donguy* [1994] by the generally lower SSS (confirmed by in-situ data in Figure 1) and the further northward extension in the 1000 km wide longitude band between  $60^\circ\text{--}50^\circ\text{W}$ . The plume area exceeds  $10^6 \text{ km}^2$  when the wind speed has a monthly minimum of 3 m/s in September, 2011 (Figure 2c). After September the winds strengthen as the northeasterly trades reappear and, consistent with the *Dessier and Donguy* [1994] climatology, the area of the plume decreases perceptibly (in part due to stronger wind mixing), reaching a minimum in January–March, 2012 (Figure 2c).

[12] As tropical storm Katia approached the plume from the east (August 30–September 2, Figures 3a and 3d) its cool wake was relatively weak  $<0.5^\circ\text{C}$  (comparing the week prior to the week following Figures 3c and 3f). The oceanic response changed on September 2 as the storm entered the region of the plume and rapidly strengthened to Category 2. SST under the hurricane initially increased to  $28.5^\circ\text{C}$ , while the cooling intensified to  $\sim 1^\circ\text{C}$  (Figures 3c and 3f). Hurricane-induced mixing caused a 1–2 psu rise in SSS in the plume (Figures 3b and 3e) and Katia continued to strengthen to Category 4 by September 4. SST cooling rapidly amplified to  $\sim 2^\circ\text{C}$  as the hurricane left the plume area (Figures 3c and 3f).

[13] The strong SSS increase in hurricane wake within the plume (Figures 3 and 4) is explained by an erosion of the BL. This is evident by Argo profiles collected within the plume (Figure 5, #1, #3; see also auxiliary material, Figure S3, for location #2) that indicate the presence of shallow, about 15 m deep mixed layer overlying the halocline. Mixed layer salinity is lower by 2 to 4 psu than the water beneath. This shallow haline stratification is destroyed by hurricane-forced entrainment (mixed layer deepening and upwelling), which is stronger on the right side of hurricane eye. Although the hurricane strengthened further along the trajectory, the SSS change is much weaker there corresponding to weak vertical salinity stratification outside the plume (Figure 5, #8 and Figure S3, #7).

[14] On the left side of the trajectory there is an area of SSS decrease (Figure 4) sampled by Argo #4 and #5. In contrast to the increase in SSS within the plume where the BL is eroded, the surface (down to 30 m, Figure 5 #5) adjacent to the northwestern corner of the plume is 1 psu fresher after the passage of hurricane. The decrease in salinity implies an addition of 1 m of freshwater, much larger than could have come from direct rainfall. The most likely explanation is freshwater advection from the plume with some additional contribution due to direct rainfall.

[15] Magnitude of SSS increase in the haline wake (about 1.5 psu, Figure 4) agrees with the vertical salinity change of 3 to 4 psu (found in the vertical profiles within the plume, Figure 5 #1 and #3) for mixing penetrating down to twice the initial halocline depth. SSS changes observed by Aquarius and SMOS qualitatively well agree (Figure 4) suggesting that satellite sensing of SSS is a mature technique for strong signals  $>1 \text{ psu}$ .

[16] The thermal wake is detectable along the entire hurricane track and gradually intensifies with the intensifying hurricane, but the haline wake is mostly confined to the plume (Figure 6). In the week following hurricane passage the SST cooling is less pronounced in the plume where SST remains warmer by  $0.5^\circ\text{C}$  than SST outside (Figure 6b). The shallower vertical stratification of salinity acts to reduce SST



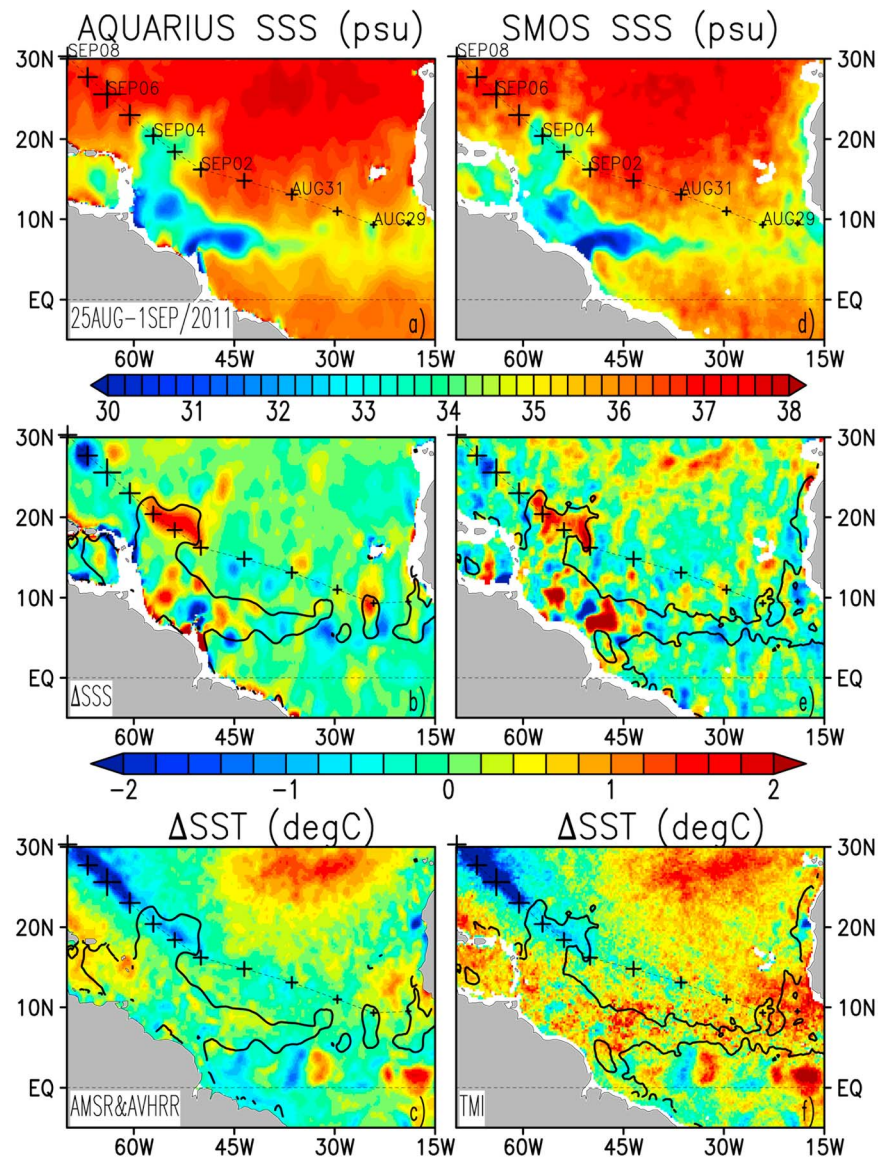


**Figure 3.** (a) AQUARIUS and (d) SMOS SSS before hurricane Katia. Crosses are the hurricane daily position at 00:00UTC with size scaled between 20kt and 120kt of maximum sustained winds (from NHC analysis). (b, e) SSS and (c, f) SST differences after (5–10 SEP/2011) minus before (25AUG–1SEP/2011) the hurricane passage. 35 psu contour before the passage of Katia is overlain. The differences are color-scaled between  $-2$  and  $2$ . Land-contaminated coastal data are blanked.

cooling (because extra work required to mix the BL), and thus impacts hurricane growth by weaker negative feedback, an interpretation consistent with *Sengupta et al.* [2008], *Wang et al.* [2011], and *Balaguru et al.* [2012].

#### 4. Summary and Conclusions

[17] About 68% of hurricanes that finally reached category 5 have crossed the Amazon/Orinoco plume [*Ffield, 2007*] where the presence of BL can enhance their growth rate by 50% [*Balaguru et al., 2012*]. Here we present a case study of the passage of hurricane Katia over the plume for which an

extensive array of remote sensed and in situ observations are available, in particular new SSS from SMOS and Aquarius. A similarly strong haline wake event was detected with SMOS alone following hurricane Igor in September, 2010 ([www.esa.int/esaEO/SEMJFHWX7YG\\_index\\_1.html#subhead3](http://www.esa.int/esaEO/SEMJFHWX7YG_index_1.html#subhead3)). The availability of SSS from both SMOS and Aquarius reinforces these first observations and demonstrates spatial and temporal patterns of hurricane-BL interactions in an unprecedented manner. We find that both Igor and Katia forced SSS changes  $>1$  psu over an area exceeding  $10^5$  km<sup>2</sup>. These abrupt changes last and have implications for SSS climate, since SSS is not damped like SST.

**Figure 4.** (a) Aquarius and (b) SMOS SSS difference ( $\Delta$ SSS) between after (5–10 SEP/2011) minus before (25AUG–1SEP/2011) the passage of Katia. Location of Argo profiles before ('o') and after ('+') the passage. Bold solid and dashed are 35 psu contour before and after the passage, respectively. Land-contaminated coastal data are blanked.

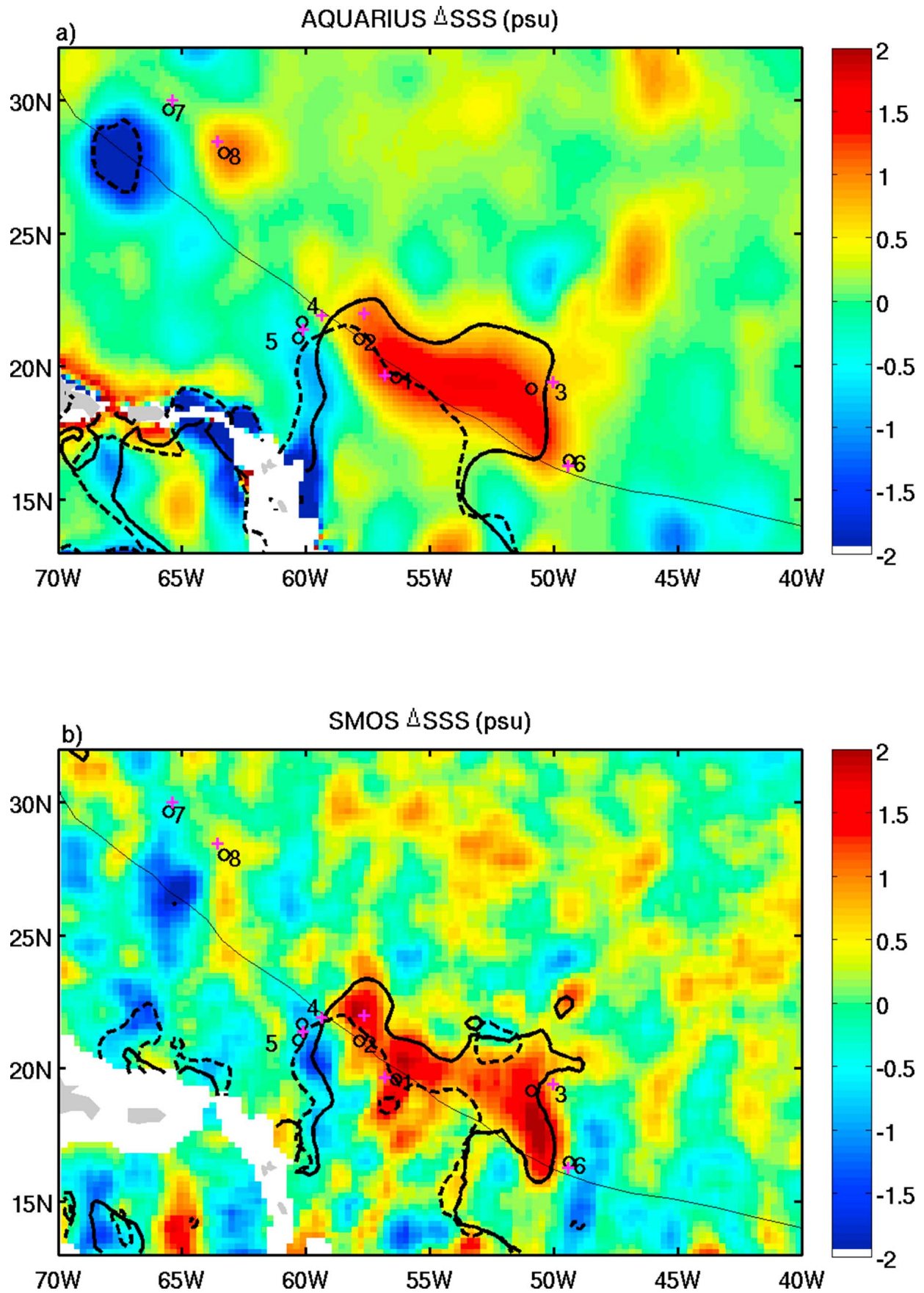
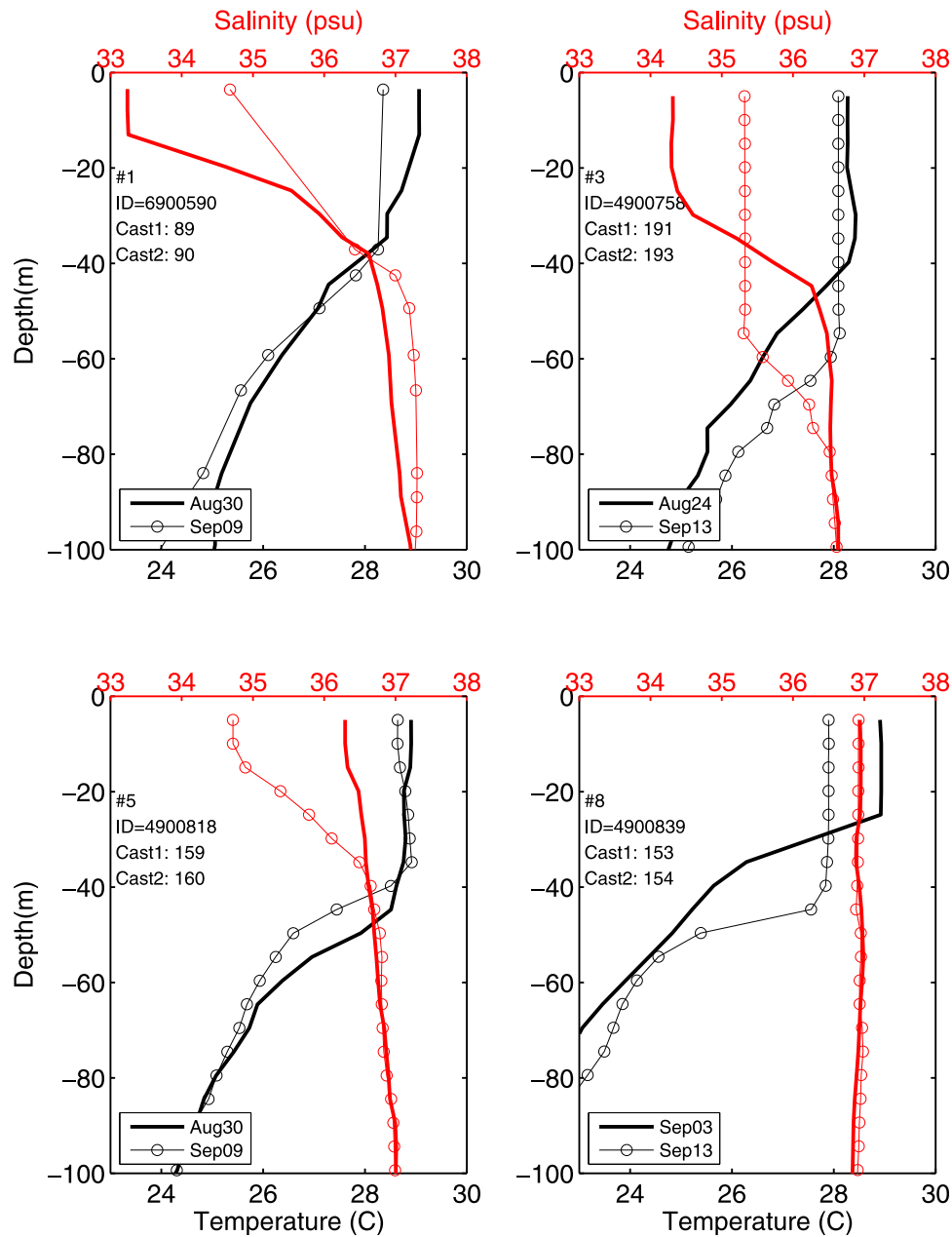


Figure 4



**Figure 5.** Argo profiles of temperature and salinity before (bold) and after (open circles) the passage of Katia (see Figure 4 for profile locations and auxiliary material for the rest of profiles).

[18] These observations confirm that over the plume a uniform density mixed layer is shallower than uniform temperature layer because of stable halocline, acting to inhibit cooling and vertical mixing. Under an intense hurricane the halocline, which is above the thermocline, is mixed first. This produces a SSS wake that is by a few psu saltier than initial SSS in the plume. From space-time diagrams of SSS and SST along the hurricane track we find that haline wake develops only within the plume and is associated with at least  $0.5^{\circ}\text{C}$  weaker SST cooling than outside the plume. This difference in SST cooling is explained by additional work required to mix the BL. Thus BL leads to a reduction in hurricane-induced surface cooling that favors hurricane development, as the resulting elevated SST and high evaporation enhance the hurricane's maximum potential intensity.

[19] The geographic location and seasonality of the Amazon/Orinoco plume make hurricane overpasses a not-infrequent occurrence. Indeed, the expansion of the plume in August-September coincides with the peak of the production of Cape Verde hurricanes, a group which includes many of the most intense (Category 4–5) hurricanes. Thus the results presented here strongly suggest that the salinity stratification role in mixed layer dynamics should be taken into account when forecasting hurricane growth over the plume. The availability of satellite SSS from Aquarius and SMOS along with in situ ARGO measurements is critical to making such model improvements practical.

[20] **Acknowledgments.** This research was supported by NASA (NNX12AF68G, NNX09AF34G), ESA/ESRIN (AO/1-6704/11/I-AM), CNES support to CATDS, and Russian Government (11.G34.31.0078). TSG data are provided by ESA's SMOS Cal/Val effort supported by the



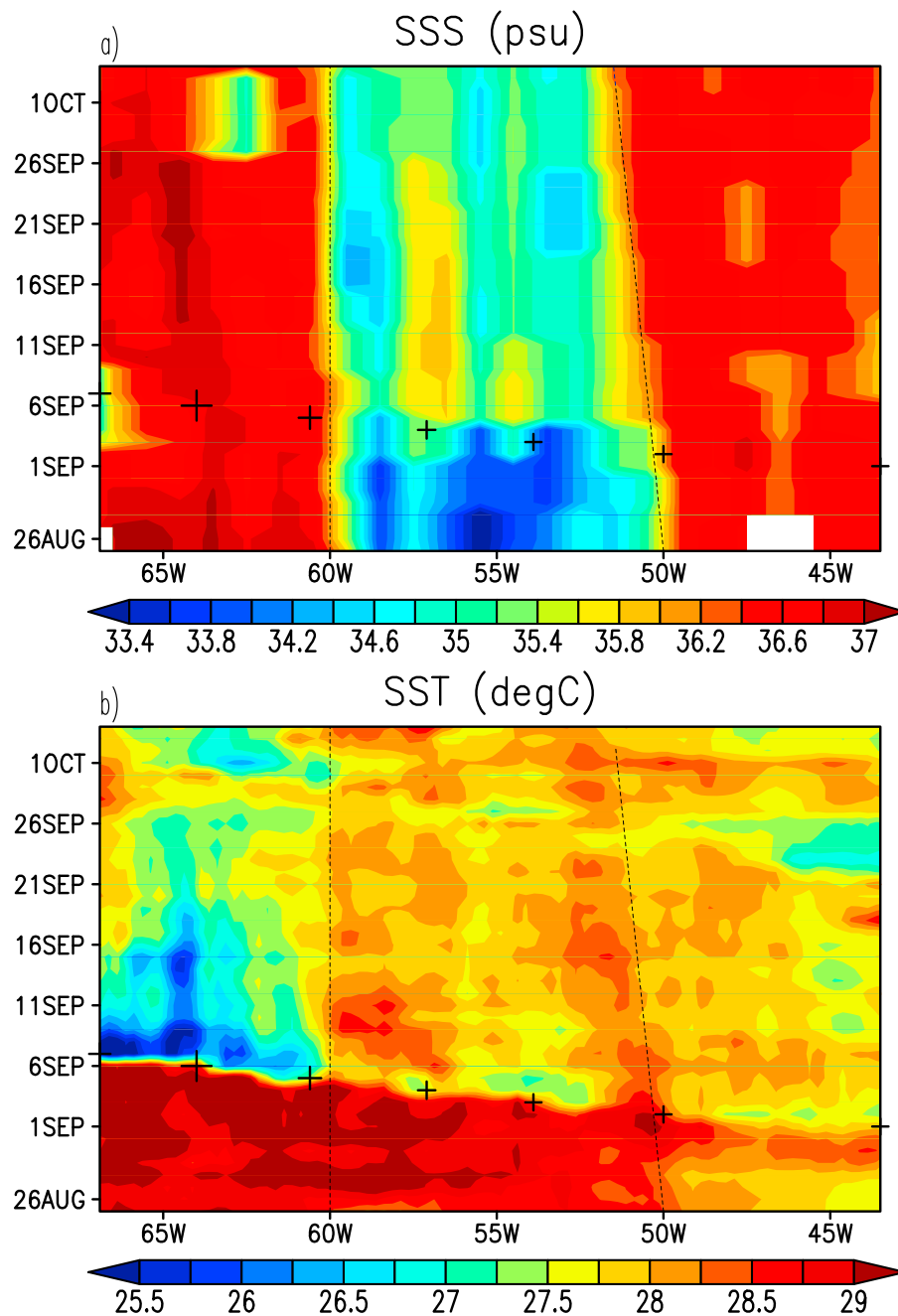


**Figure 6.** Temporal diagram of (a) weekly running mean AQUARIUS SSS and (b) SST along the hurricane track (see Figure 5). Hurricane positions are overlain (see Figure 3 for marker scale). Fresh pool is encompassed by dashed lines. X-axis presents longitude along the track.

CNES/TOSCA program and are collected from merchant vessels by the SSS observatory supported by IRD and INSU. TSG data were prepared by Denis Diverrès and Gaël Alory. We thank Da-Lin Zhang for comments on an earlier version of this manuscript.

[21] The Editor thanks two anonymous reviewers for their assistance in evaluating this paper.

## References

- Balaguru, K., P. Chang, R. Saravanan, L. R. Leung, Z. Xu, M. Li, and J.-S. Hsieh (2012), Ocean barrier layers' effect on tropical cyclone intensification, *Proc. Natl. Acad. Sci. U. S. A.*, *109*, 36, 14343–14347, doi:10.1073/pnas.1201364109.
- Bender, M. A., and I. Ginis (2000), Real-case simulations of hurricane-ocean interaction using a high-resolution coupled model: Effects on hurricane intensity, *Mon. Weather Rev.*, *128*, 917–946, doi:10.1175/1520-0493(2000)128<0917:RCSOHO>2.0.CO;2.
- Bentamy, A., and D. Croize-Fillon (2012), Gridded surface wind fields from Metop/ASCAT measurements, *Int. J. Remote Sens.*, *33*, 1729–1754, doi:10.1080/01431161.2011.600348.
- Dessier, A., and J. R. Donguy (1994), The sea surface salinity in the tropical Atlantic between 10°S and 30°N—Seasonal and interannual variations (1977–1989), *Deep Sea Res., Part 1*, *41*, 81–100, doi:10.1016/0967-0637(94)90027-2.
- Ffield, A. (2007), Amazon and Orinoco River plumes and NBC rings: Bystanders or participants in hurricane events?, *J. Clim.*, *20*, 316–333, doi:10.1175/JCLI3985.1.
- Foltz, G. R., and M. J. McPhaden (2008), Seasonal mixed layer salinity balance of the tropical North Atlantic Ocean, *J. Geophys. Res.*, *113*, C02013, doi:10.1029/2007JC004178.

- Henocq, C., J. Boutin, G. Reverdin, F. Petitcolin, S. Arnault, and P. Lattes (2010), Vertical variability of near-surface salinity in the tropics: Consequences for L-band radiometer calibration and validation, *J. Atmos. Oceanic Technol.*, *27*, 192–209, doi:10.1175/2009JTECHO670.1.
- Hu, C., E. T. Montgomery, R. W. Schmitt, and F. E. Muller-Karger (2004), The dispersal of the Amazon and Orinoco River water in the tropical Atlantic and Caribbean Sea: Observation from space and S-PALACE floats, *Deep Sea Res., Part II*, *51*, 1151–1171.
- Lagerloef, G., et al. (2008), The Aquarius/SAC-D mission: Designed to meet the salinity remote-sensing challenge, *Oceanography*, *21*, 68–81, doi:10.5670/oceanog.2008.68.
- Lagerloef, G. (2012), Satellite mission monitors ocean surface salinity, *Eos Trans. AGU*, *93*(25), 233, doi:10.1029/2012EO250001.
- Lagerloef, G., F. Wentz, S. Yueh, H.-Y. Kao, G. C. Johnson, and J. M. Lyman (2012), Aquarius satellite mission provides new, detailed view of sea surface salinity, in *State of the Climate in 2011*, *Bull. Am. Meteorol. Soc.*, vol. 93, pp. S70–S71, Boston, Mass.
- Lee, T., G. Lagerloef, M. M. Gierach, H.-Y. Kao, S. Yueh, and K. Dohan (2012), Aquarius reveals salinity structure of tropical instability waves, *Geophys. Res. Lett.*, *39*, L12610, doi:10.1029/2012GL052232.
- Lentz, S. J. (1995), Seasonal variations in the horizontal structure of the Amazon plume inferred from historical hydrographic data, *J. Geophys. Res.*, *100*, 2391–2400, doi:10.1029/94JC01847.
- Lumpkin, R., and Z. Garraffo (2005), Evaluating the decomposition of tropical Atlantic drifter observations, *J. Atmos. Oceanic Technol.*, *22*, 1403–1415, doi:10.1175/JTECH1793.1.
- McPhaden, M. J., G. R. Foltz, T. Lee, V. S. N. Murty, M. Ravichandran, G. A. Vecchi, J. Vialard, J. D. Wiggert, and L. Yu (2009), Ocean–atmosphere interactions during Cyclone Nargis, *Eos Trans. AGU*, *90*(7), 53, doi:10.1029/2009EO070001.
- Mignot, J., A. Lazar, and M. Lacarra (2012), On the formation of barrier layers and associated vertical temperature inversions: A focus on the northwestern tropical Atlantic, *J. Geophys. Res.*, *117*, C02010, doi:10.1029/2011JC007435.
- Pailler, K., B. Bourlès, and Y. Gouriou (1999), The barrier layer in the western tropical Atlantic Ocean, *Geophys. Res. Lett.*, *26*, 2069–2072, doi:10.1029/1999GL900492.
- Price, J. F. (1981), Upper ocean response to a hurricane, *J. Phys. Oceanogr.*, *11*, 153–175, doi:10.1175/1520-0485(1981)011<0153:UORTAH>2.0.CO;2.
- Reul, N., J. Tenerelli, J. Boutin, B. Chapron, F. Paul, E. Brion, F. Gaillard, and O. Archer (2012a), Overview of the first SMOS sea surface salinity products. Part I: Quality assessment for the second half of 2010, *IEEE Trans. Geosci. Remote Sens.*, *50*, 1636–1647, doi:10.1109/TGRS.2012.2188408.
- Reul, N., J. Tenerelli, B. Chapron, D. Vandemark, Y. Quilfen, and Y. Kerr (2012b), SMOS satellite L-band radiometer: A new capability for ocean surface remote sensing in hurricanes, *J. Geophys. Res.*, *117*, C02006, doi:10.1029/2011JC007474.
- Reverdin, G., S. Morisset, J. Boutin, and N. Martin (2012), Rain-induced variability of near sea-surface T and S from drifter data, *J. Geophys. Res.*, *117*, C02032, doi:10.1029/2011JC007549.
- Reynolds, R. W., T. M. Smith, C. Liu, D. B. Chelton, K. S. Casey, and M. G. Schlax (2007), Daily high-resolution-blended analyses for sea surface temperature, *J. Clim.*, *20*, 5473–5496, doi:10.1175/2007JCLI1824.1.
- Roemmich, D., and the Argo Steering Team (2009), Argo: The challenge of continuing 10 years of progress, *Oceanography*, *22*, 46–55, doi:10.5670/oceanog.2009.65.
- Salisbury, J., D. Vandemark, J. Campbell, C. W. Hunt, D. Wisser, N. Reul, and B. Chapron (2011), Spatial and temporal coherence between Amazon River discharge, salinity, and light absorption by colored organic carbon in western tropical Atlantic surface waters, *J. Geophys. Res.*, *116*, C00H02, doi:10.1029/2011JC006989.
- Saunders, M. A., and A. S. Lea (2008), Large contribution of sea surface warming to recent increase in Atlantic hurricane activity, *Nature*, *451*, 557–560, doi:10.1038/nature06422.
- Sengupta, D., B. R. Goddalahundi, and D. S. Anitha (2008), Cyclone-induced mixing does not cool SST in the post-monsoon north Bay of Bengal, *Atmos. Sci. Lett.*, *9*, 1–6, doi:10.1002/asl.162.
- Shay, L. K., G. J. Goni, and P. G. Black (2000), Effects of a warm oceanic feature on hurricane Opal, *Mon. Weather Rev.*, *128*, 1366–1383, doi:10.1175/1520-0493(2000)128<1366:EOAWOF>2.0.CO;2.
- Vizy, E. K., and K. H. Cook (2010), Influence of the Amazon/Orinoco Plume on the summertime Atlantic climate, *J. Geophys. Res.*, *115*, D21112, doi:10.1029/2010JD014049.
- Wang, X.-D., G. Han, Y.-Q. Qi, and W. Li (2011), Impact of barrier layer on typhoon-induced sea surface cooling, *Dyn. Atmos. Oceans*, *52*, 367–385, doi:10.1016/j.dynatmoce.2011.05.002.
- Yoo, J.-M., and J. A. Carton (1990), Annual and interannual variation of the freshwater budget in the tropical Atlantic and Caribbean Sea, *J. Phys. Oceanogr.*, *20*, 831–845, doi:10.1175/1520-0485(1990)020<0831:AAIVOT>2.0.CO;2.
- Zhu, T., and D.-L. Zhang (2006), The impact of the storm-induced SST cooling on hurricane intensity, *Adv. Atmos. Sci.*, *23*, 14–22, doi:10.1007/s00376-006-0002-9.